



Study on Coupling Effect and Dynamic Behavior of Double Bubbles Rising Process

Lanxin Gong, Changhong Peng^(✉), and Zhenze Zhang

School of Nuclear Science and Technology, University of Science and Technology of China,
Hefei, Anhui, China

{lenovomax, desolate}@mail.ustc.edu.cn, pengch@ustc.edu.cn

Abstract. Gas-liquid two-phase flow widely exists in nuclear energy engineering, in which bubble movement and deformation are critical problems. Because the activity of bubbles in the fluid is a very complex physical process, and the movement process is a flow field-bubble coupling process, which has strong non-linearity and unsteady, the relevant research is usually based on experiments and simulation.

We built a medium-sized experimental device to generate double bubbles with different sizes and characteristic numbers and recorded the motion trajectory with a high-speed camera. We developed and improved the image processing method to obtain high-quality bubble motion information and realized a good capture of bubble shape and rotation.

The experimental results show that in the two bubbles rising successively, the trailing bubble is affected by the trailing field of the leading bubble, and the bubble velocity, relative distance, deformation rate, and other parameters change accordingly. In addition, through simulation, we get the interaction mechanism of the bubbles under experimental conditions. The results show that the coupling leads to flow field velocity and pressure changes, which explains the experimental results. The research results are helpful for a thorough understanding of the law of bubble movement and provide empirical data support for developing a thermal-hydraulic model.

Keywords: Bubble rising experiment · Bubble coupling · Gas-liquid two-phase flow

1 Introduction

Since the last century, researchers have carried out a lot of research on bubble motion from the aspects of theory, experiment, and numerical simulation [1–3].

There are various forms of bubble movement. For the free bubble, if it is affected by the rigid wall, it will not only deform the bubble interface but also change its original motion state, mainly including the movement of the bubble away from the wall, the movement of the bubble close to the wall, and the bounce movement of the bubble along the wall. For free-space bubbles, it is relatively simple, mainly showing a zigzag and spiral rise. Predecessors have also carefully studied the rise of single bubble and bubble

chains and obtained the laws of bubble terminal velocity, bubble deformation, and other motion parameters in some cases.

Generally speaking, in the presence of a wall, bubbles are affected laterally by the wall attraction (lift pointing towards the wall) and the wall repulsion (lift pointing away from the wall). When bubbles are affected by repulsive force and attraction, they appear in a zigzag motion. In the longitudinal direction, bubbles are usually affected by lift, drag, additional mass force, and film-induced force, regardless of whether the wall exists. Because the growth and movement of bubbles are very complex, involving the mass conversion between two phases and the energy transfer between three phases, the growth and movement mechanism of bubbles have not been fully understood. In addition, as a unique flow field boundary, bubbles have an important influence on the dynamics of other bubbles around them, making the problem more complex. When two bubbles rise in parallel, the smaller spacing will lead to bubble fusion; When bubbles rise one after another, the wake of the leading bubble will cause the bubbles that follow to rise faster. These coupling effects significantly change the bubble distribution and two-phase contact area and affect the heat and mass transfer performance.

Clift et al. [1] studied the change of bubble shape and drew the bubble phase diagram. It was found that bubbles with a diameter of less than 1.3 mm remained spherical, and the shape of large bubbles would be the oval and spherical cap. Duineveld [4] studied the floating characteristics of bubbles with a diameter of 0.33–1 mm in purified water, explored the equilibrium velocity and shape coefficient obtained by bubbles and the relationship between Weber number We , and found that the maximum Weber number that can float in a stable shape and velocity does not exceed 3.2. Raymond and Rosant [5], Zenit [6], and Magnaudet [6] use different liquids or add different proportions of chemicals to the water to change the density, viscosity, surface tension coefficient, and other parameters of the fluid and explore the changing laws and internal relations of physical quantities such as bubble resistance coefficient, shape, and buoyancy under different We and Re . Wu and Gharib [7] found that the bubbles with a diameter of 0.1–0.2 cm were spherical or ellipsoidal in the floating process. When the bubble volume was constant, the bubbles with high rising velocity were generally ellipsoidal; In addition, the upward floating path of bubbles with a diameter less than 1.5 mm is a straight line. When the bubble size is larger, the upward floating path of bubbles will be Z shaped or spiral-shaped.

As for the interaction between two bubbles, Duineveld's experimental research shows that if the horizontal approach velocity of bubbles is the characteristic velocity when We are less than 0.18, the two bubbles will become a single bubble. When the bubble radius is less than 0.7 mm, the impact velocity of the two bubbles is always tiny, so the possibility of bubbles fusion is high. When We are less than the critical value, the two bubbles after springing could collide again. Sanada et al. [8] conducted an experimental study on the interaction between two horizontal bubbles and found that when re exceeds a specific range, the two bubbles attract each other. After the collision, there may be two cases of fusion or bounce-off. If the bounce-off occurs, the bubble floating speed will be reduced by about 50% due to vortex shedding and other reasons. The occurrence of different phenomena is related to Re and We . It is pointed out that the critical We are about 2, and the critical Re is related to the Morton number Mo .

As for the terminal velocity, it depends on the bubble shape and is related to the Eotvos number, Reynolds number, and Morton number. Wallis [9], Grace [10], Jamialahmadi [11], Bozzano [12], Sung-Hoon Park [13], and others proposed a series of correlations based on experiments. As for the application of final velocity, it is widely used in system analysis programs (such as RELAP5 [14]) to determine the selection of flow patterns, heat transfer correlations, etc.

2 Experimental Equipment

The central part of the experimental device is a $30 \times 30 \times 40$ cm acrylic water tank. In the tank, the rubber tube and Ruhr joint are connected with the flat head stainless steel needle tube; Outside the tank, the micro air pump and the gas pipe are connected with the flow regulating valve and the micro syringe. When bubbles need to be generated, open the air pump, control the gas flow rate by adjusting the flow regulating valve, and change the bubble size by changing the diameter of the syringe needle in the cylinder. As shown in Fig. 1, when recording bubbles from the front, a strip-shaped parallel light source is set at the back of the cylinder; When shooting bubbles on the left side, place a rectangular light source on the right side of the cylinder, as shown in Fig. 1. The high-speed camera is supported by stable support and is connected to the computer, which can process the captured images in real-time. To simplify the subsequent image processing, we record the bubbles in the dark environment and keep the white LED light source so that the captured image has a white background and the bubble itself is black. In the experiment, we set the camera to shoot at the frame rate of 500 fps.

Table 1. Experimental group and needle diameter

Serial number	1	2	3	4	5	6
OD/mm	2.42	1.86	1.29	3.46	2.78	4.00
Number of experiments	21	23	17	14	16	12

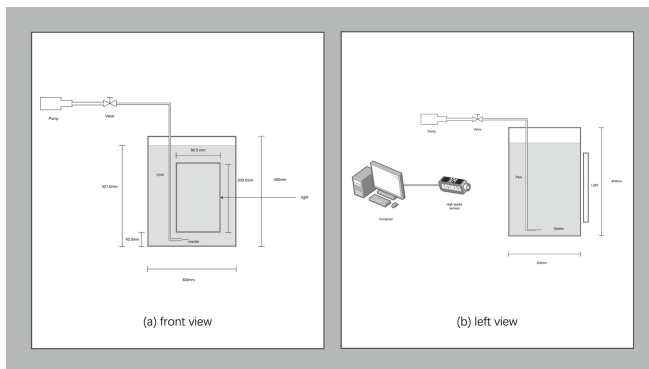


Fig. 1. Schematic diagram of the experimental device

Under the above experimental conditions, we generated a free-rising single bubble and a continuous rising double bubble. It is noted that it is difficult for parallel bubbles to combine into a single bubble due to the influence of initial needle diameter and spacing. Several experiments were carried out under each working condition to generate single and double bubbles repeatedly, and the rising motion of bubbles was photographed with a camera. The bubble video with high contrast, slight noise, and within the width of the light source is selected to study the law of motion and deformation. We used the following diameter needles to generate bubbles of different sizes (Table 1).

3 Image Processing

We use mature image processing technology, and the Python program and OpenCV library are selected to develop the corresponding image processing program. Image processing mainly includes four steps: preprocessing, image segmentation, contour clustering, and feature extraction.

3.1 Preprocessing

Preprocessing includes image frame clipping, keyframe interval selection, gray level processing, binarization processing, Gaussian filtering, etc. The image frame is cut to retain the image of the experimental section, and the width is slightly wider than the width of the light source. Keyframe interval selection mainly selects the video interval of the bubble rising process. Gray processing prepares for binarization, and binarization processes the image into a two-color image according to the threshold. Gaussian filtering can filter out part of the image noise.

3.2 Image Segmentation

Image segmentation is mainly to identify bubbles and the surrounding environment. The Canny operator processes the image to obtain the bubble boundary, and then the contour data is obtained using the *findcontours* function in OpenCV.

3.3 Contour Clustering

For some single bubble cases, due to the uniformity of the light source and the light refraction caused by the bubble movement, the bubble contour is divided into several parts. For the double bubble case, the attribution relationship of the bubble contour needs to be considered, so the contour clustering analysis code needs to be developed. The sub-function is used to calculate the center of a single outline and the number of data points. Then the center points representing each contour are divided according to the distance (such as Manhattan distance, Euclidean distance, etc.), which are mainly divided into two categories, namely, the corresponding leading bubble and the trailing bubble (for the case of a single bubble, it can be considered that the top bubble and the trailing bubble overlap), as shown in Fig. 2. In addition, it is often necessary to eliminate interference

profiles. The elimination of the interference profile depends on the shape factor, which is defined as follows.

$$K = \frac{P^2}{4\pi S} \quad (1.1)$$

where P is the contour perimeter and S is the contour area.

3.4 Feature Extraction

According to the results of segmentation and clustering, the feature parameters such as bubble centroid are extracted, and the saved data are output for subsequent data processing. The pictures processed in four steps are shown in Fig. 2.

We define the center of mass and velocity of the bubble as follows,

$$X = \frac{\sum_{i=1}^{i=N} x_i}{N} \quad (1.2)$$

$$Y = \frac{\sum_{i=1}^{i=N} y_i}{N} \quad (1.3)$$

$$v_x^t = \frac{X^{t+1} - X^t}{\Delta t} s \quad (1.4)$$

$$v_y^t = \frac{Y^{t+1} - Y^t}{\Delta t} s \quad (1.5)$$

where x_i, y_i are coordinates of all pixels within the bubble contour. X and Y are obtained bubble centroid coordinates. s is the ratio of true distance to unit pixel. Δt is the time difference between two frames.

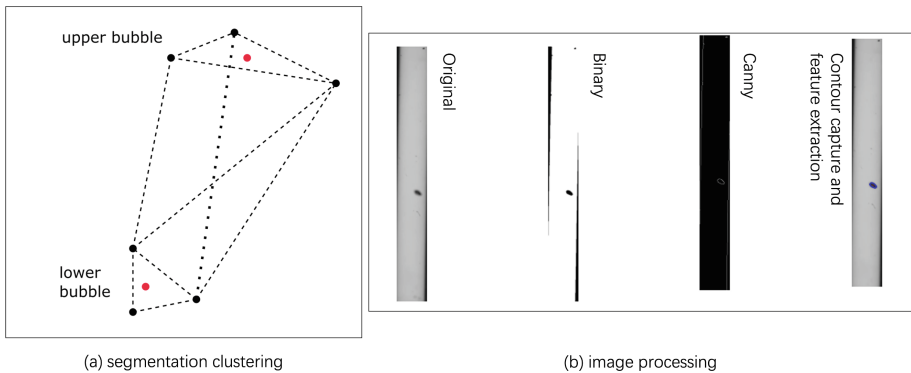


Fig. 2. Schematic diagram of segmentation clustering algorithm and image processing flow

The deformation degree and equivalent volume diameter are related to the long-axis b and short-axis a (assuming the bubble shape is elliptical). The deformation degree of the bubble can also be expressed by the aspect ratio, while the volume diameter could be defined as,

$$E = \frac{b}{a} \quad (1.6)$$

$$d_e = \sqrt[3]{b^2 a} \quad (1.7)$$

During the experiment, we also extracted dimensionless parameters, which are defined as follows,

$$\text{Re} = \frac{\rho v d_e}{\mu} \quad (1.8)$$

$$\text{Eo} = \frac{d_e^2 (\rho_l - \rho_g) g}{\sigma} \quad (1.9)$$

$$\text{We} = \frac{v^2 d_e \rho_l}{\sigma} \quad (1.10)$$

where ρ is the density, v is the velocity of the bubble, g is the gravitational acceleration, σ is the surface tension.

4 Result and Analysis

4.1 Trajectory and Deformation

The trajectory of bubble motion is different under different equivalent volume diameters. As shown in Fig. 3, the captured trajectory shows that almost all bubbles are zigzagging or spiraling. When the equivalent diameter is less than 5 mm, the bubble is easier to twist.

Generally speaking, the larger the equivalent diameter, the more serious the deformation. Generally speaking, the larger the equivalent diameter, the more serious the deformation. According to the definition, when K and E are large, the deviation from the circle is big, and the deformation is large.

We get the deformation coefficients under different diameters, as shown in Fig. 4. It can be seen that when K is used as a parameter to characterize deformation, it conforms to the previous discussion. However, when E is taken as a parameter, the deformation relationship of the leading bubble is broken. This is because the ratio of long and short axes can only reflect the length relationship in the direction of the two main axes. Therefore, we propose to use K instead of E to represent the degree of deformation. In addition, we can also see that the deformation degree of the lower bubble increases under the influence of the flow field behind the forward bubble.

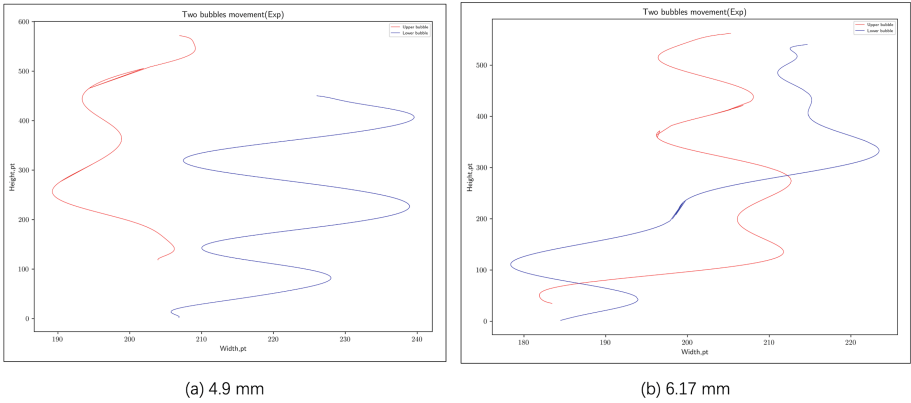


Fig. 3. Centroid locus (red line: top bubble blue line: bottom bubble)

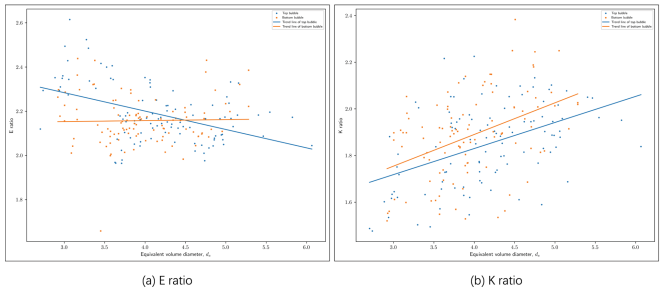


Fig. 4. K and E under different equivalent diameters(E on the left, K on the right)

4.2 Instantaneous Parameters

We place the light source in the middle and rear part of the bubble movement and record the changes in velocity, relative distance, and dimensionless number with time. As shown in Fig. 5 and Fig. 6, the speed in the x -direction under different equivalent diameters presents periodic variation characteristics. The speed in the y -direction fluctuates up and down in the mean value.

It is observed that the x -direction distance between the two bubbles fluctuates around the mean value, while the y -direction distance may fluctuate or decrease. This is related to the relative velocity of the two bubbles. The dimensionless parameters also present periodic fluctuations, mainly related to the changes in equivalent diameter and speed.

4.3 Terminal Velocity

In the field of nuclear engineering, people are concerned about the change of terminal velocity with equivalent diameter.

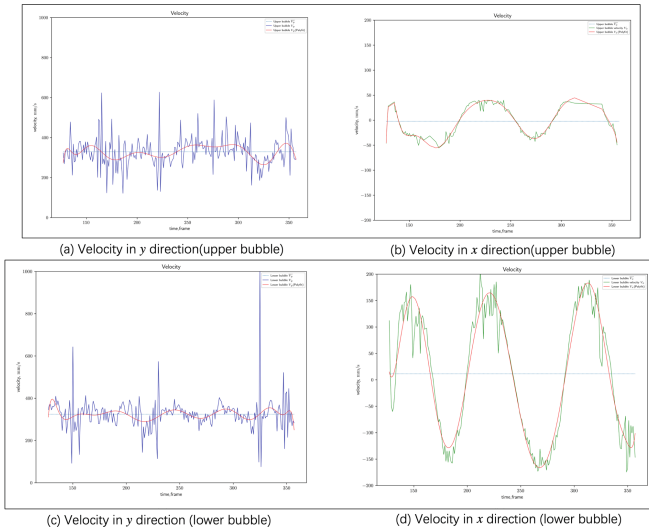


Fig. 5. Bubble velocity in *x-y* direction

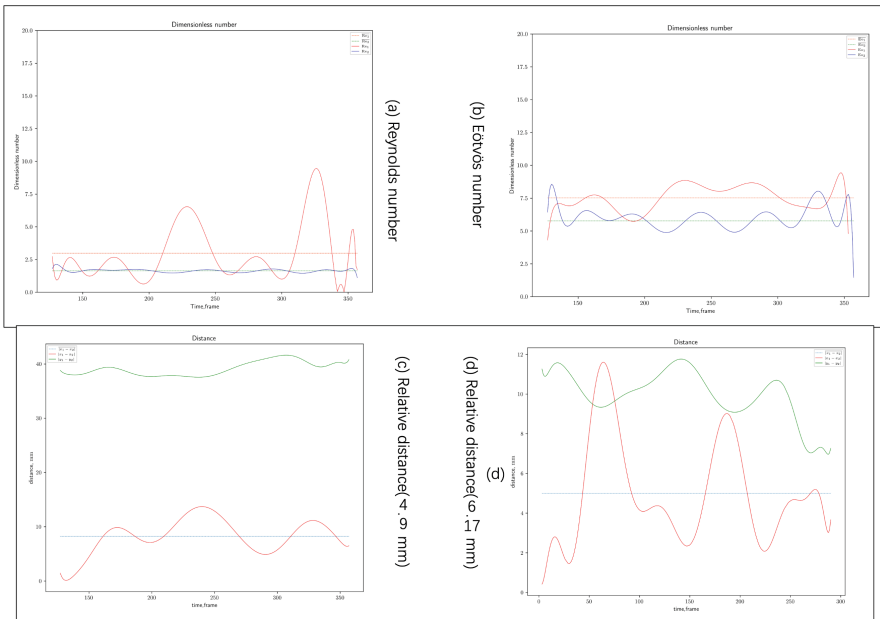


Fig. 6. Schematic diagram of time variation of dimensionless parameters and relative distance under different equivalent diameters

As shown in Fig. 7, we used a series of correlations for prediction and found that the Wallis correlation had a significant error, Davis and Taylor[15, 16] correlation were slightly better, and Park correlation and Clift[1] correlation were close in trend. We

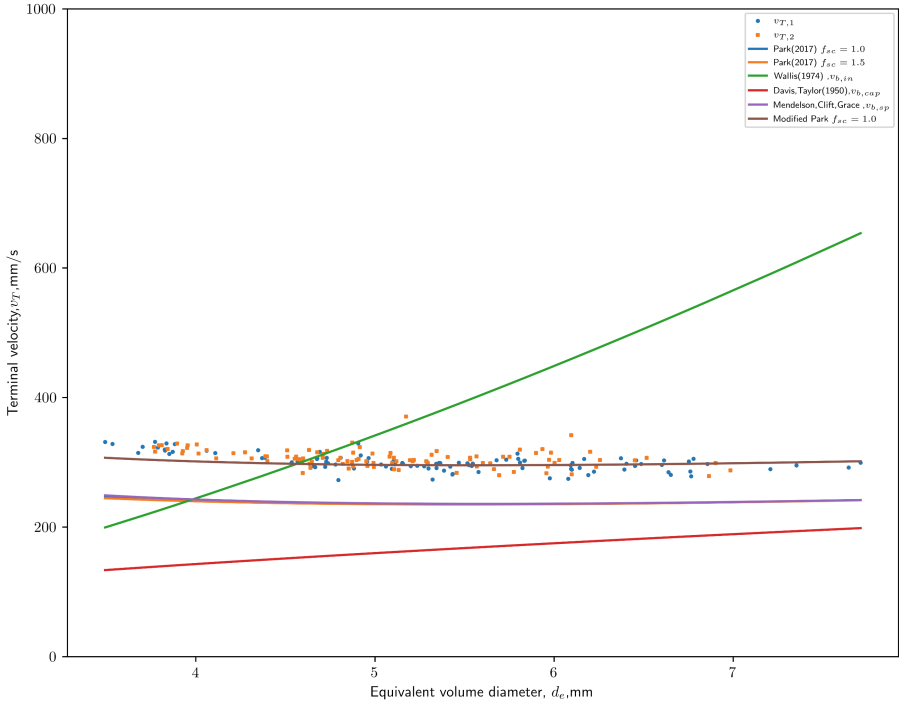


Fig. 7. Bubble terminal velocity under different equivalent diameters and fitting correlations

corrected the Park[13] correlation by adding a velocity offset term $v_{offset} = 0.06$ m/s, and found that the predicted results were in good agreement with the experiment.

$$v_{b,in} = 0.14425g^{5/6} \left(\frac{\rho_L}{\mu_L} \right)^{2/3} d_e^{3/2} \tag{1.11}$$

$$v_{b,sp} = \sqrt{\frac{2.14\sigma_L}{\rho_L d_e} + 0.505gd_e} \tag{1.12}$$

$$v_{b,cap} = 0.721\sqrt{gd_e} \tag{1.13}$$

$$v_{b,park} = \frac{1}{\sqrt{\frac{1}{v_{b,sp}^2} + \frac{1}{v_{b,non-sp}^2}}} = \frac{1}{\sqrt{f_{sc}^2 \left(\frac{144\mu_L^2}{g^2 \rho_L^2 d_e^4} + \frac{\mu_L^{4/3}}{0.14425^2 g^{5/3} \rho_L^{4/3} d_e^3} \right) + \frac{1}{\frac{2.14\sigma_L}{\rho_L d_e} + 0.505gd_e}}} \tag{1.14}$$

4.4 Numerical Simulation

In this paper, the VOF multiphase flow model in Fluent software is used to simulate the bubble flow field. A rectangular space of 10×40 cm is taken, the two sides of the surface boundary are set as symmetry surfaces, the top is set as a pressure outlet, and the surface tension coefficient of water at room temperature and pressure is taken using Harkins' empirical formula. The flow field was obtained by simulating the forward bubble with an equivalent diameter of 5 mm as shown in Fig. 8 and Fig. 9. It can be seen that under the influence of bubble-field coupling, the transverse velocity of the flow field (x -direction) changes significantly, and the fluid's transverse velocity and the flow field's longitudinal velocity (y -direction) increases, which will affect the next bubbles. We can see that the change in the transverse velocity of the flow field will strengthen or limit the transverse movement of the next bubbles (depending on the direction of the bubble movement), and the increase in the longitudinal velocity of the flow field will accelerate the next bubbles.

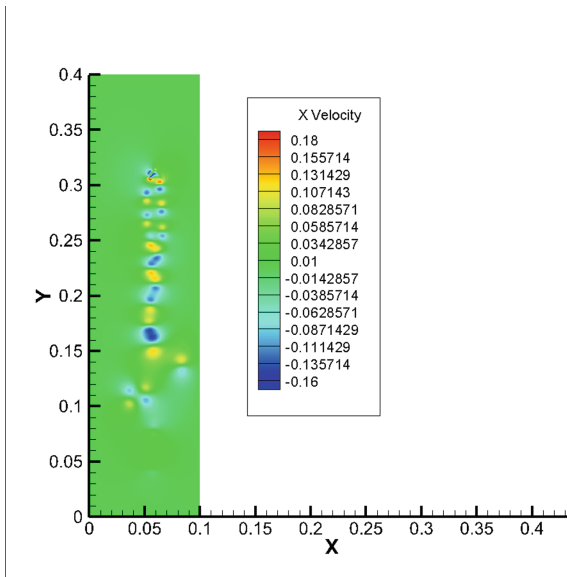


Fig. 8. Bubble flow field velocity (x direction)

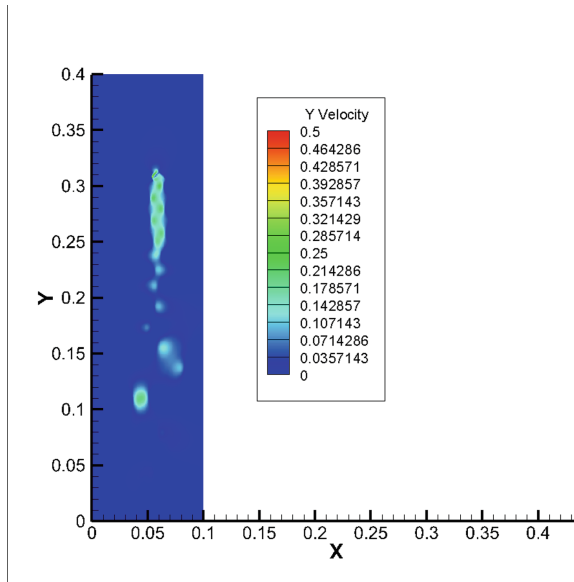


Fig. 9. Bubble flow field velocity (y direction)

5 Conclusions

To sum up, by generating double bubbles in different states, we developed an image processing program based on OpenCV to study the motion and deformation law of double bubbles with varying diameters of equivalent. We get the following conclusions: 1) the shape coefficient K can better reflect the shape change during bubble rising than the aspect ratio E . 2) The instantaneous parameters of two bubbles show periodic characteristics. 3) Both simulations and experiments show that the change of the tail flow field caused by the movement and deformation of the first bubble will affect the subsequent bubble and then change its movement. 4) The bottom bubbles were slightly accelerated by the flow field behind the top bubbles. We modified the Park correlation and achieved a good prediction of the terminal velocity of the experiment.

References

1. Clift, R., Grace, J.R., Weber, M.E.: Bubbles, Drops, and Particles. Dover Publications (2005)
2. Feng, Z.G., Michaelides, E.E.: Interparticle forces and lift on a particle attached to a solid boundary in suspension flow. *Phys. Fluids* **14**(1), 49–60 (2002)
3. Zhang, A.M., Cui, P., Cui, J., Wang, Q.X.: Experimental study on bubble dynamics subject to buoyancy. *J. Fluid Mech.* **776**, 137–160 (2015)
4. Duineveld, P.C.: The rise velocity and shape of bubbles in pure water at high Reynolds number. *J. Fluid Mech.* **292**, 325–332 (1995)
5. Raymond, F., Rosant, J.M.: A numerical and experimental study of the terminal velocity and shape of bubbles in viscous liquids. *Chem. Eng. Sci.* **55**(5), 943–955 (2000)

6. Zenit, R., Magnaudet, J.: Path instability of rising spheroidal air bubbles: a shape-controlled process. *Phys. Fluids* **20**(6), 061702 (2008)
7. Wu, M., Gharib, M.: Experimental studies on the shape and path of small air bubbles rising in clean water. *Phys. Fluids* **14**(7), L49–L52 (2002)
8. Sanada, T., Sato, A., Shirota, M., Watanabe, M.: Motion and coalescence of a pair of bubbles rising side by side. *Chem. Eng. Sci.* **64**(11), 2659–2671 (2009)
9. Wallis, G.B.: The terminal speed of single drops or bubbles in an infinite medium. *Int. J. Multiphase Flow* **1**(4), 491–511 (1974)
10. Grace, J.R.: Shapes and velocities of bubbles rising in infinite liquids. *Trans. Inst. Chem. Eng.* **51**, 116–120 (1973)
11. Jamialahmadi, M., Müller-Steinhagen, H.: Effect of superficial gas velocity on bubble size, terminal bubble rise velocity and gas hold-up in bubble columns. *Dev. Chem. Eng. Miner. Process.* **1**(1), 16–31 (1993)
12. Bozzano, G., Dente, M.: Shape and terminal velocity of single bubble motion: a novel approach. *Comput. Chem. Eng.* **25**(4–6), 571–576 (2001)
13. Park, S.H., Park, C., Lee, J., Lee, B.: A simple parameterization for the rising velocity of bubbles in a liquid pool. *Nucl. Eng. Technol.* **49**(4), 692–699 (2017)
14. Fletcher, C., Schultz, R.: RELAP5/MOD3 code manual. Nuclear Regulatory Commission, Washington, DC (United States) (1992)
15. Davis, R.E., Acrivos, A.: The influence of surfactants on the creeping motion of bubbles. *Chem. Eng. Sci.* **21**(8), 681–685 (1966)
16. Davies, R.M., Taylor, G.I.: The mechanics of large bubbles rising through extended liquids and through liquids in tubes. *Proc. Roy. Soc. Lond. Ser. A Math. Phys. Sci.* **200**(1062), 375–390 (1950)

Open Access This chapter is licensed under the terms of the Creative Commons Attribution 4.0 International License (<http://creativecommons.org/licenses/by/4.0/>), which permits use, sharing, adaptation, distribution and reproduction in any medium or format, as long as you give appropriate credit to the original author(s) and the source, provide a link to the Creative Commons license and indicate if changes were made.

The images or other third party material in this chapter are included in the chapter's Creative Commons license, unless indicated otherwise in a credit line to the material. If material is not included in the chapter's Creative Commons license and your intended use is not permitted by statutory regulation or exceeds the permitted use, you will need to obtain permission directly from the copyright holder.

